A Hybrid S_N-Diffusion Method for Molten Salt Reactor Control Rod Modeling

M&C 2025

Sun Myung Park, The University of Texas at Austin
Kathryn D. Huff, University of Illinois Urbana-Champaign
Madicken Munk, Oregon State University

April 28, 2025

ILLINOIS

Outline

Outline

Control Rods in MSRs

Control rods provide a means of controlling the fission rate in nuclear reactors.

- Facilitate reactor start-up, shut-down, or load-following operations
- Consist of highly neutron-absorbing materials such as boron or gadolinium

Control rods are also important for licensing and safety characterization.

⇒ **It is important to characterize control rod effects in all relevant transient scenarios.**

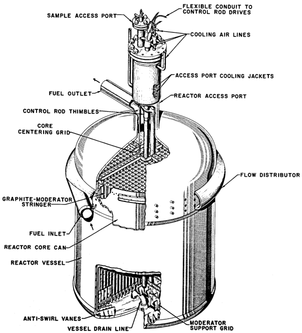

Figure 1: Centrally located control rods in the Molten Salt Reactor Experiment (MSRE) [1]

Control Rod Modeling

Control rods induce highly anisotropic neutron fluxes and steep flux gradients in their vicinity.

Control Rod Modeling Dilemma

- Neutron diffusion, P_1, and SP_N methods perform poorly near control rod regions due to the highly anisotropic neutron fluxes and steep flux gradients
- High-fidelity neutron transport methods remain too computationally expensive for routine time-dependent multiphysics simulations

Control Rod Modeling

Control rods induce highly anisotropic neutron fluxes and steep flux gradients in their vicinity.

Control Rod Modeling Dilemma

- Neutron diffusion, P_1, and SP_N methods perform poorly near control rod regions due to the highly anisotropic neutron fluxes and steep flux gradients
- High-fidelity neutron transport methods remain too computationally expensive for routine time-dependent multiphysics simulations

Objective

Develop a hybrid S_N-diffusion method for accurate control rod modeling in time-dependent MSR analyses.

Outline

Moltres for MSR Multiphysics Modeling

What is Moltres?
Moltres [2] is an open-source, MOOSE-based multiphysics application for modeling MSRs

Software Capabilities for MSR Modeling

- Multigroup neutron diffusion solver
- Temperature reactivity feedback by interpolating temperature-dependent group constant data
- delayed neutron precursor (DNP) drift coupling with flow modeling
- Out-of-core DNP decay
- Couples with MOOSE modules for thermal-hydraulics modeling

Existing Methods in Literature

Transport-Correction Techniques For Neutron Diffusion-Based Solvers

Techniques for augmenting the neutron diffusion method (or equivalent low-order equations) with corrections derived from neutron transport:

- Ronen method [3, 4, 5]
- Multilevel quasi-diffusion method [6, 7, 8]
- Multischeme transport method [9]
- Hybrid transport-diffusion method [10, 11]

These techniques generally require:

- High-order neutron transport solver
- Corrective terms for the neutron diffusion equations
- Boundary coupling scheme (for spatial domain decomposition)

Hybrid S_N-Diffusion Method

Method Overview

- Applies the discrete ordinates (S_N) method to a small subregion around a control rod to generate corrections for the neutron diffusion equation
- Limits computationally expensive S_N calculations to small subdomains
- Retains the computational efficiency of the neutron diffusion method
- Applies an adaptive algorithm to smooth flux gradients near the S_N-diffusion interface

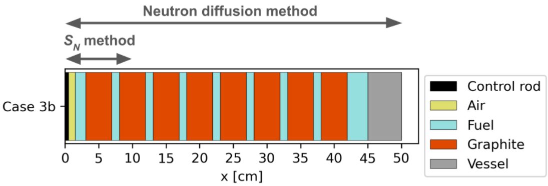

Figure 2: Illustration of the problem domains of the S_N and neutron diffusion methods in an example 1-D problem.

Hybrid S_N-Diffusion Method

Multigroup Discrete Ordinates S_N Neutron Transport Equations

The multigroup S_N equations defined on the 3-D spatial domain $\mathcal{D}$ and 2-D unit sphere angular domain $\mathcal{S}$ is:

$$\hat{\Omega} \cdot \nabla \Psi_g(\vec{r}, \hat{\Omega}, t) + \Sigma_{t,g} \Psi_g(\vec{r}, \hat{\Omega}, t) = \sum_{g'=1}^{G} \int_{\mathcal{S}} \Sigma_s^{g' \to g}(\hat{\Omega}' \to \hat{\Omega}) \Psi_{g'}(\vec{r}, \hat{\Omega}', t) d\hat{\Omega}' + \frac{1}{4\pi} \frac{\chi_{p,g}(1-\beta)}{k} \sum_{g'=1}^{G} \nu \Sigma_{f,g'} \phi_{g'}(\vec{r}, t) \quad (1)$$

with boundary conditions:

$$\Psi_g(\vec{r}, \hat{\Omega}) = \Psi_g^{\text{inc}}(\vec{r}, \hat{\Omega}) + \alpha_g^s \Psi_g(\vec{r}, \hat{\Omega}_r) \text{ on } \vec{r} \in \partial\mathcal{D} \text{ and } \hat{\Omega} \cdot \hat{n}_b < 0, \quad (2)$$

where

$$\Psi_g^{\text{inc}} = \text{incident surface source in group } g,$$
$$\alpha_g^s = \text{specular reflectivity on } \partial\mathcal{D} \text{ for group } g,$$
$$\hat{\Omega}_r = \hat{\Omega} - 2(\hat{\Omega} \cdot \hat{n}_b)\hat{n}_b = \text{reflection angle},$$
$$\hat{n}_b = \text{outward unit normal vector on the boundary.}$$

Hybrid S_N-Diffusion Method

Self-Adjoint Angular Flux (SAAF) Formulation of the Multigroup S_N Equations

Second-order linear neutron transport equation derived by obtaining the analytical solution of angular flux and substituting it back into the S_N equations.

Implementation Details

- Implemented with finite element method (FEM)
- Compatible with the efficient and scalable Hypre-BoomerAMG preconditioning
- Uses a modified formulation to handle $1/\Sigma_{t,g}$ factor in near-void regions (similar to Streamline-Upwind/Petrov Galerkin (SUPG) stabilization scheme) [12]
- Level-symmetric quadrature set for angular discretization (up to S_{18})
- Nonlinear diffusion acceleration scheme [12]

Hybrid S_N-Diffusion Method

Multigroup Neutron Diffusion Equations

$$-\nabla \cdot D_g \nabla \phi_g + \Sigma_g^r \phi_g = \sum_{g' \neq g}^{G} \Sigma_{g' \to g}^s \phi_{g'} + \frac{\chi_{p,g} (1 - \beta)}{k} \sum_{g'=1}^{G} \nu \Sigma_{g'}^f \phi_{g'} \qquad (3)$$

Traditionally, D_g is determined through region-wide neutron interaction tallies in high-fidelity neutron transport simulations as follows:

$$D_g = \frac{1}{3\Sigma_{t,g}} \quad \text{(isotropic)} \qquad (4)$$

$$D_g = \frac{1}{3\Sigma_{tr,g}} = \frac{1}{3\left(\Sigma_{t,g} - \Sigma_{s1,g}\right)} \quad \text{(linearly anisotropic)} \qquad (5)$$

where

$$\Sigma_{tr} = \text{macroscopic transport cross section}$$

Hybrid S_N-Diffusion Method

Drift Correction Scheme

This scheme arises from adding a drift term $(\vec{D}_g \cdot \nabla\phi_g)$ [12] to the neutron diffusion equations:

$$\vec{D}_g = \frac{\sum_{d=1}^{N_d} w_d \left(\tau_g \hat{\Omega}_d \hat{\Omega}_d \cdot \nabla \Psi_{g,d} + \left(\tau_g \Sigma_{t,g} - 1\right) \hat{\Omega}_d \Psi_{g,d} - \tau_g \sum_{g'=1}^{G} \Sigma_{s,1}^{g' \to g} \hat{\Omega}_d \Psi_{g',d} - D_g \nabla \Psi_{g,d}\right)}{\sum_{d=1}^{N_d} w_d \Psi_{g,d}}, \quad (6)$$

$$\gamma_g = \frac{\sum_{\hat{\Omega}_d \cdot \hat{n}_b > 0} w_d |\hat{\Omega}_d \cdot \hat{n}_b| \Psi_{g,d}}{\sum_{d=1}^{N_d} w_d \Psi_{g,d}}. \quad (7)$$

The drift term also provides pointwise corrections to the neutron diffusion equations. This formulation is derived from the SAAF-S_N equations by integrating over the angular domain and eliminating terms shared by the neutron diffusion equations.

Hybrid S_N-Diffusion Method

S_N Subsolver Boundary Conditions

For the hybrid S_N-diffusion method to converge, it requires appropriate boundary conditions for the S_N subproblem.
The P_1 approximation for evaluating the neutron angular flux along the discrete ordinates $\hat{\Omega}_d$ of the S_N angular quadrature set is:

$$\begin{aligned}\Psi_{g,d} &\approx \frac{1}{4\pi}\left(\phi_g^{\text{diff}} + 3\hat{\Omega}_d \cdot \vec{J}_g^{\text{diff}}\right) \\ &= \frac{1}{4\pi}\left(\phi_g^{\text{diff}} - 3\hat{\Omega}_d \cdot D_g \nabla \phi_g^{\text{diff}}\right) \qquad (8)\end{aligned}$$

Therefore, the boundary source term for the S_N subsolver is:

$$\Psi_{g,d}^{\text{inc}} = \frac{1}{w}\left(\phi_g^{\text{diff}} - 3\hat{\Omega}_d \cdot D_g \nabla \phi_g^{\text{diff}}\right) \qquad (9)$$

where w is the sum of weights of the level-symmetric quadrature set.

Hybrid S_N-Diffusion Method Algorithm

Legend:

V_0: Full problem domain

V_1: Problem subdomain containing control rod region

$\vec{D}_g^{(i)}$: drift correction parameter in the i-th iteration

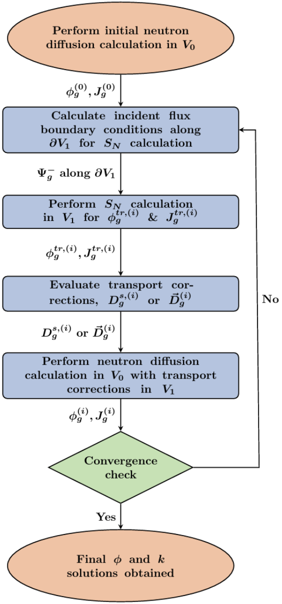

Correction Region (V_1) and Buffer Region

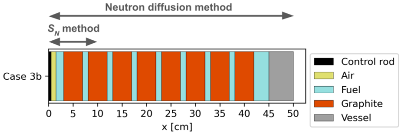

Figure 4: 1-D geometry for Case 3b.

- The approximate S_N boundary conditions will yield some flux deviations near the correction region boundary.
- This affects transport correction parameters near the boundary.

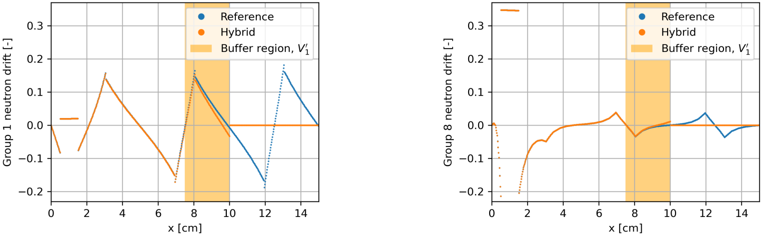

Figure 5: The reference and hybrid drift ($\vec{D}_g$) distributions for group 1 and 8 calculated from S_8 and S_8-diffusion simulations. The correction subregion V_1 spans $x = 0$ cm to $x = 10$ cm.

Correction Region (V_1) and Buffer Region

A natural/intuitive criterion for the location of the buffer region cutoff boundary would be wherever the components of the drift correction variable $\vec{D}_g$ is zero, i.e., wherever the components change signs.

1. At points where the $\vec{D}_g$ components are zero, the flux is approximately isotropic along the axes corresponding to the components.
2. This choice preserves the smoothness of the neutron flux gradient.

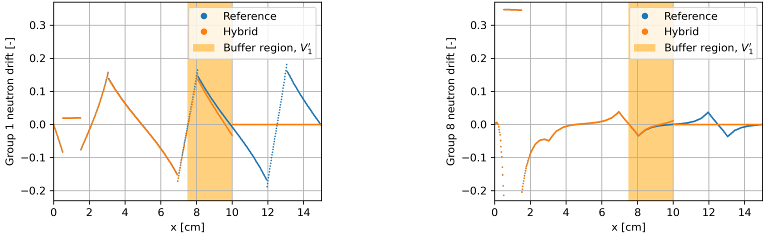

Figure 6: The reference and hybrid drift ($\vec{D}_g$) distributions for group 1 and 8 calculated from S_8 and S_8-diffusion simulations. The correction subregion V_1 spans $x = 0$ cm to $x = 10$ cm.

Hybrid S_N-Diffusion Method

Numerical Implementation

The SAAF-S_N and hybrid S_N-diffusion method with the drift correction scheme were implemented on Moltres.

- Preconditioned Jacobian-free Newton-Krylov (PJFNK) solver [13]
- Hypre-BoomerAMG (Algebraic multigrid) preconditioning [14]
- MultiApp and Transfers systems from MOOSE for iterative coupling and data transfers
- Supporting material and utility C++ classes for loading group constant data and performing angular quadrature calculations

1-D MSRE Neutronics Model Geometries

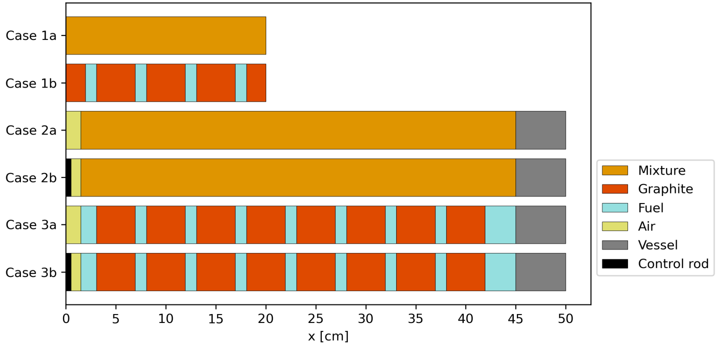

Figure 7: Geometries of the 1-D test cases. The material labeled "mixture" represents a homogeneous mixture of fuel and graphite at a ratio of 22.5%-77.5% by volume. All geometries have reflective boundary conditions on the boundary at $x = 0$ cm. The right-side boundaries are reflective for Cases 1a and 1b, and vacuum for Cases 2a, 2b, 3a, and 3b.

1-D MSRE Neutronics Modeling Approach

1-D Neutronics Model Setup

- Material compositions derived from the MSRE design
- Reduced gadolinium content in control rod to 0.35 wt%
- Eight neutron energy groups
- Group constants generated using OpenMC with up to 2nd-order Legendre expansions of scattering matrices
- Uniform temperature at 900 K

Table 1: Neutron energy group structure in this work. Originally devised by Jaradat [15].

Group	Upper energy bound [eV]
1	2.000×10^{7}
2	1.353×10^{6}
3	6.734×10^{4}
4	9.118×10^{3}
5	1.487×10^{2}
6	4.000×10^{0}
7	6.250×10^{-1}
8	8.000×10^{-2}

1-D MSRE Neutronics Modeling Approach

1-D Neutronics Model Numerical Solvers

All 1-D cases ran on each of the following numerical solvers:

1. OpenMC in continuous energy mode (OpenMC-CE)
2. OpenMC in multigroup mode (OpenMC-MG)
3. Neutron diffusion method (Moltres)
4. S_8 method (Moltres)
5. Hybrid S_8-diffusion method (Moltres)

Reactivity & Reactivity Difference

$$\text{Reactivity } \rho \equiv \frac{k_{\text{eff}} - 1}{k_{\text{eff}}}. \tag{10}$$

$$\Delta\rho = \rho_1 - \rho_2 = \frac{k_{\text{eff},1} - k_{\text{eff},2}}{k_{\text{eff},1} k_{\text{eff},2}}. \tag{11}$$

Outline

1-D MSRE Neutronics Simulation Results

1-D Neutronics Model Reactivity Results

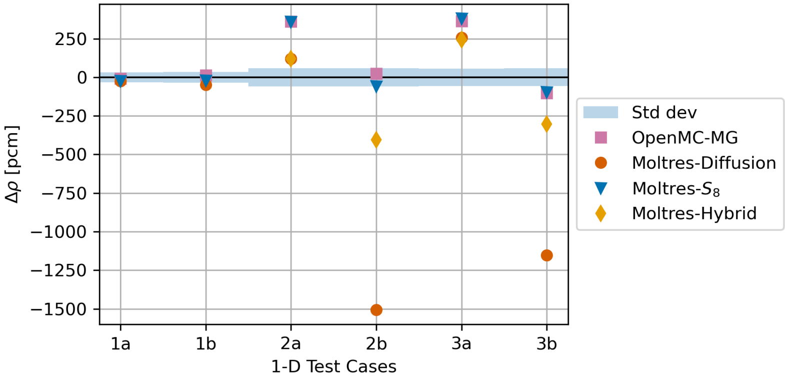

Figure 8: Difference in reactivity ρ of all neutronics methods investigated relative to OpenMC-CE.

1-D MSRE Neutronics Simulation Results

1-D Neutronics Model Control Rod Worth Results

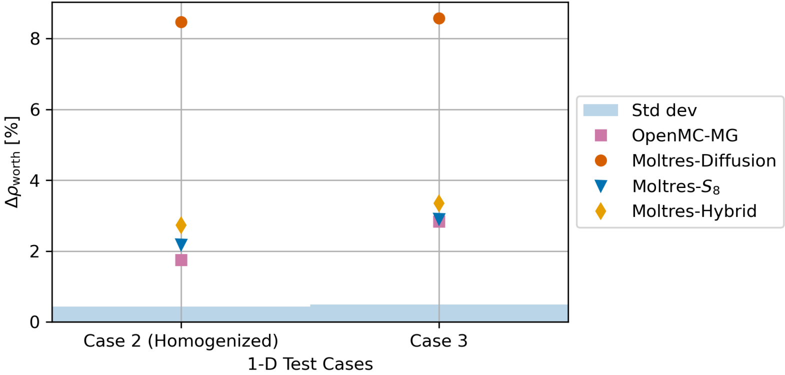

Figure 9: Percentage difference in rod worth for Cases 2 and 3 of all neutronics methods investigated relative to OpenMC-CE.

1-D MSRE Neutronics Simulation Results

Case 3b Geometry

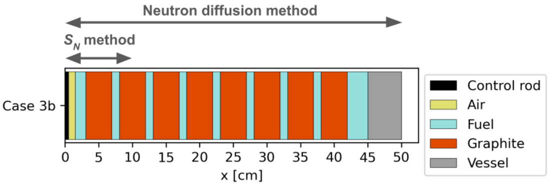

Figure 10: Geometry of 1-D Case 3b.

1-D MSRE Neutronics Simulation Results

Case 3b Neutron Flux Distributions

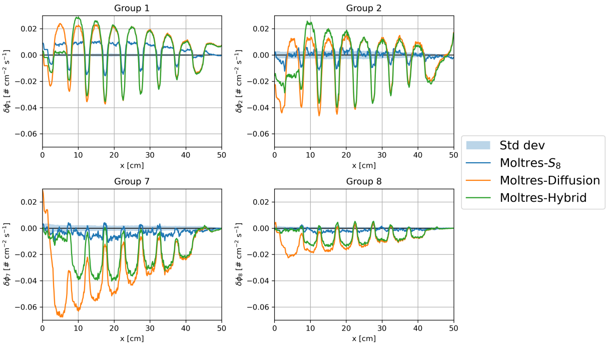

Figure 11: Absolute difference in neutron group flux distributions for Case 3b from Moltres-S_8, Moltres-diffusion, and Moltres-hybrid relative to OpenMC-MG.

The hybrid method provides more accurate flux estimates than the neutron diffusion method near $x = 0$ cm where the control rod is situated.

1-D MSRE Neutronics Simulation Results

Impact of Correction Subregion Sizes on Rod Worth

- Rod worth estimates vary non-monotonically with increasing correction subregion size.
- Rod worth estimates remain within 0.2% of the S_8 method rod worth.
- The hybrid method produces accurate rod worth estimates as long as the correction region size is kept consistent.

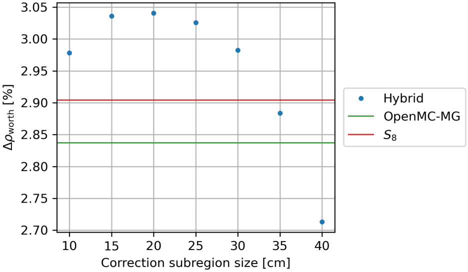

Figure 12: Percentage difference in rod worth from the hybrid method relative to OpenMC-CE for Cases 3a and 3b with different correction subregion sizes.

1-D MSRE Neutronics Simulation Results

Relaxing the S_N Convergence Tolerance, ϵ_{tol}

- Transport correction parameters converge faster than scalar flux in the S_N subsolver.
- Relaxing the S_N subsolver convergence tolerance would provide computational savings.
- The hybrid method exhibits superlinear ($q = 1.333$) convergence in k with respect to the S_8 convergence tolerance value.

Table 2: Number of outer iterations in hybrid method calculations of Case 3b for a given set of convergence tolerance values imposed on the S_8 subsolver.

Tolerance value, ϵ_{tol}	10^{-8}	10^{-7}	10^{-6}	10^{-5}	10^{-4}	10^{-3}
No. of outer iterations	3	3	3	2	2	1

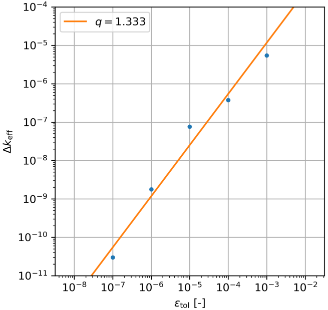

Figure 13: k_{eff} error estimates of Case 3b for a range of S_8 subsolver convergence tolerance values relative to the reference k_{eff} value when $\epsilon_{tol} = 10^{-8}$.

Outline

Conclusion

Hybrid S_N-Diffusion Method for time-dependent control rod modeling

- Developed a hybrid S_N-diffusion method for control rod modeling in time-dependent simulations.
- The method involves generating drift correction parameters around the control rod region using the S_N method.
- The transport-corrected subregion size adaptively changes in response to the drift correction distributions.
- 1-D results show the hybrid method improves rod worth and flux estimates over the diffusion method.

Extensions to this work

- Extend the hybrid S_N-diffusion method to 2-D and 3-D models. (Completed)
- Demonstrate time-dependent reactivity-initiated transients. (Completed)
- Improve computational performance of the hybrid S_N-diffusion method.

References I

[1] R. C. Robertson, "MSRE DESIGN AND OPERATIONS REPORT. PART I. DESCRIPTION OF REACTOR DESIGN," English, Oak Ridge National Lab., Tenn., Tech. Rep. ORNL-TM-728, Jan. 1965. (visited on 03/27/2019).

[2] A. Lindsay, G. Ridley, A. Rykhlevskii, and K. Huff, "Introduction to Moltres: An application for simulation of Molten Salt Reactors," en, *Annals of Nuclear Energy*, vol. 114, pp. 530–540, Apr. 2018. (visited on 01/08/2018).

[3] Y. Ronen, "Accurate Relations between the Neutron Current Densities and the Neutron Fluxes," en, *Nuclear Science and Engineering*, vol. 146, no. 2, pp. 245–247, Feb. 2004. [Online]. Available: https://www.tandfonline.com/doi/full/10.13182/NSE04-A2407 (visited on 07/19/2022).

[4] D. Tomatis, R. Gross, and E. Gilad, "On the Ronen Method in Simple 1-D Geometries for Neutron Transport Theory Solutions," *Journal of Computational and Theoretical Transport*, vol. 50, no. 2, pp. 134–157, Feb. 2021. [Online]. Available: https://doi.org/10.1080/23324309.2020.1843496 (visited on 07/20/2022).

[5] R. Gross, J. Cufe, D. Tomatis, and E. Gilad, "Comprehensive investigation of the Ronen method in slab geometry," *Nuclear Engineering and Technology*, vol. 55, no. 2, pp. 734–748, Feb. 2023. (visited on 06/14/2024).

[6] V. Y. Gol'din, "A quasi-diffusion method of solving the kinetic equation," *USSR Computational Mathematics and Mathematical Physics*, vol. 4, no. 6, pp. 136–149, Jan. 1964. [Online]. Available: https://www.sciencedirect.com/science/article/pii/0041555364900850 (visited on 02/28/2024).

[7] A. Tamang and D. Y. Anistratov, "A Multilevel Projective Method for Solving the Space-Time Multigroup Neutron Kinetics Equations Coupled with the Heat Transfer Equation," *Nuclear Science and Engineering*, vol. 177, no. 1, pp. 1–18, May 2014. (visited on 04/03/2024).

[8] A. J. Reynolds and T. S. Palmer, "An Analysis of Transport Effects in Steady-State Simulation of the Molten Salt Reactor Experiment," *Nuclear Science and Engineering*, vol. 197, no. 1, pp. 45–73, Jan. 2023. [Online]. Available: https://doi.org/10.1080/00295639.2022.2097565 (visited on 02/17/2023).

[9] Y. Wang, S. Schunert, M. DeHart, R. Martineau, and W. Zheng, "Hybrid PN-SN with Lagrange multiplier and upwinding for the multiscale transport capability in Rattlesnake," *Progress in Nuclear Energy*, Special Issue on the Physics of Reactors International Conference PHYSOR 2016: Unifying Theory and Experiments in the 21st Century, vol. 101, pp. 381–393, Nov. 2017. [Online]. Available: https://www.sciencedirect.com/science/article/pii/S0149197017300653 (visited on 05/01/2024).

References II

[10] D. Y. Anistratov and N. D. Stehle, "Computational transport methodology based on decomposition of a problem domain into transport and diffusive subdomains," *Journal of Computational Physics*, vol. 231, no. 24, pp. 8009–8028, Oct. 2012. [Online]. Available: https://www.sciencedirect.com/science/article/pii/S0021999112003154 (visited on 04/30/2024).

[11] N. D. Stehle, D. Y. Anistratov, and M. L. Adams, "A hybrid transport-diffusion method for 2D transport problems with diffusive subdomains," *Journal of Computational Physics*, vol. 270, pp. 325–344, Aug. 2014. (visited on 04/30/2024).

[12] Y. Wang, H. Zhang, and R. C. Martineau, "Diffusion Acceleration Schemes for Self-Adjoint Angular Flux Formulation with a Void Treatment," *Nuclear Science and Engineering*, vol. 176, no. 2, pp. 201–225, Feb. 2014. (visited on 06/10/2024).

[13] D. A. Knoll and D. E. Keyes, "Jacobian-free Newton–Krylov methods: A survey of approaches and applications," en, *Journal of Computational Physics*, vol. 193, no. 2, pp. 357–397, Jan. 2004. [Online]. Available: http://www.sciencedirect.com/science/article/pii/S0021999103004340 (visited on 01/15/2014).

[14] hypre, *Hypre: High Performance Preconditioners*, 2022. [Online]. Available: https://llnl.gov/casc/hypre.

[15] M. Jaradat, "Development of Neutronics Analysis Capabilities for Application of Flowing Fuel Molten Salt Reactors," en, Thesis, University of Michigan, 2021. [Online]. Available: http://deepblue.lib.umich.edu/handle/2027.42/171425 (visited on 07/15/2024).

[16] M. O. Fratoni, D. Shen, J. Powers, and G. Ilas, "Molten Salt Reactor Experiment Benchmark Evaluation," English, Univ. of California, Berkeley, CA (United States), Tech. Rep. DOE-UCB-8542, Mar. 2020. [Online]. Available: https://www.osti.gov/biblio/1617123 (visited on 07/15/2021).

[17] B. Prince, S. Ball, J. Engel, P. Haubenreich, and T. Kerlin, *ZERO-POWER PHYSICS EXPERIMENTS ON THE MOLTEN-SALT REACTOR EXPERIMENT*. Jan. 1968.

Hybrid S_N-Diffusion Method: Theory

Weak Formulation of the Multigroup SAAF S_N Equations

Streaming term:

$$\sum_{g=1}^{G}\sum_{d=1}^{N_d} w_d \left(\hat{\Omega}_d \cdot \nabla \Psi^*_{g,d}, \tau_g \hat{\Omega} \cdot \nabla \Psi_{g,d} - (1 - \tau_g \Sigma_{t,g})\Psi_{g,d}\right)_{\mathcal{D}} \tag{12}$$

Collision term:

$$\sum_{g=1}^{G}\sum_{d=1}^{N_d} w_d \left(\Psi^*_{g,d}, \Sigma_{t,g}\Psi_{g,d}\right)_{\mathcal{D}} \tag{13}$$

Scattering term:

$$\sum_{g=1}^{G}\sum_{d=1}^{N_d} w_d \left(\Psi^*_{g,d} + \tau_g \hat{\Omega}_d \cdot \nabla \Psi^*_{g,d}, \sum_{g'=1}^{G}\sum_{l=0}^{L} \Sigma_{s,l}^{g' \to g} \sum_{m=-l}^{l} \frac{2l+1}{w} Y_{l,m}(\hat{\Omega}_d)\phi_{g',l,m}\right)_{\mathcal{D}} \tag{14}$$

Fission source term:

$$\sum_{g=1}^{G}\sum_{d=1}^{N_d} w_d \left(\Psi^*_{g,d} + \tau_g \hat{\Omega}_d \cdot \nabla \Psi^*_{g,d}, \frac{1}{w}\frac{\chi_{p,g}(1-\beta)}{k} \sum_{g'=1}^{G} \nu\Sigma_{f,g'}\phi_{g'}\right)_{\mathcal{D}} \tag{15}$$

Hybrid S_N-Diffusion Method: Theory

Weak Formulation of the Multigroup SAAF S_N Equations

Delayed neutron source term:

$$\sum_{g=1}^{G}\sum_{d=1}^{N_d} w_d \left(\Psi^*_{g,d} + \tau_g \hat{\Omega}_d \cdot \nabla \Psi^*_{g,d}, \frac{1}{w} \sum_{i=1}^{I} \chi_{d,g} \lambda_i C_i \right)_{\mathcal{D}} \tag{16}$$

Boundary source term:

$$\begin{cases} \sum_{g=1}^{G} \sum_{d=1}^{N_d} w_d \left(\Psi^*_{g,d}, \hat{\Omega}_d \cdot \hat{n}_b \Psi_{g,d} \right)_{\partial\mathcal{D}}, & \hat{\Omega} \cdot \hat{n}_b > 0, \vec{r} \in \partial\mathcal{D} \\ \sum_{g=1}^{G} \sum_{d=1}^{N_d} w_d \left(\Psi^*_{g,d}, \hat{\Omega}_d \cdot \hat{n}_b \Psi^{\text{inc}}_{g,d} \right)_{\partial\mathcal{D}}, & \hat{\Omega} \cdot \hat{n}_b < 0, \vec{r} \in \partial\mathcal{D} \end{cases} \tag{17}$$

Reflecting boundary term:

$$\begin{cases} \sum_{g=1}^{G} \sum_{d=1}^{N_d} w_d \left(\Psi^*_{g,d}, \hat{\Omega}_d \cdot \hat{n}_b \Psi_{g,d} \right)_{\partial\mathcal{D}}, & \hat{\Omega} \cdot \hat{n}_b > 0, \vec{r} \in \partial\mathcal{D}_s \\ \sum_{g=1}^{G} \sum_{d=1}^{N_d} w_d \left(\Psi^*_{g,d}, \hat{\Omega}_d \cdot \hat{n}_b \Psi_{g,d_r} \right)_{\partial\mathcal{D}}, & \hat{\Omega} \cdot \hat{n}_b < 0, \vec{r} \in \partial\mathcal{D}_s \end{cases} \tag{18}$$

Hybrid S_N-Diffusion Method: Theory

Weak Formulation of the Multigroup SAAF S_N Equations

Void stabilization parameter [12]:

$$\tau_g = \begin{cases} \frac{1}{c\Sigma_{t,g}} \text{ for } ch\Sigma_{t,g} \geq \varsigma \\ \frac{h}{\varsigma} \text{ for } ch\Sigma_{t,g} < \varsigma \end{cases} , \tag{19}$$

where

$$h = \text{mesh element size},$$
$$c = \text{maximum stabilization factor},$$
$$\varsigma = \text{void constant}.$$

$c = 1$ and $\varsigma = 0.5$ by default.

The SAAF-S_N equations require this stabilization scheme in near-void regions where $\Sigma_{t,g}$ is very small.

1-D Neutronics Model Mesh Convergence Tests

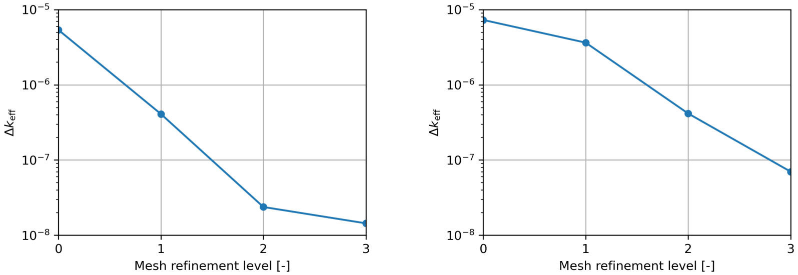

(a) Neutron diffusion method

(b) S_8 neutron transport method

Figure 14: Convergence of multiplication factor (k_{eff}) estimates for Case 3b across four levels of mesh refinement relative to the finest mesh resolution.

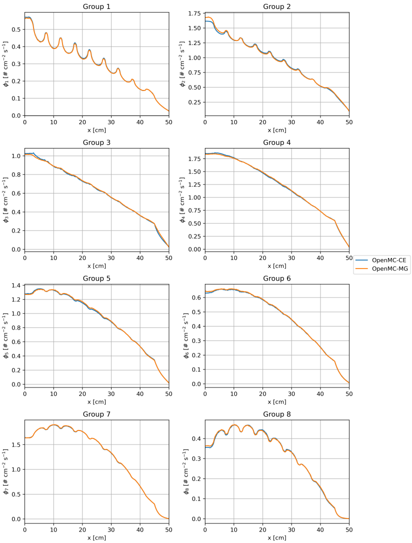

Figure 15: Case 3a neutron group flux distributions from OpenMC-CE and OpenMC-MG.

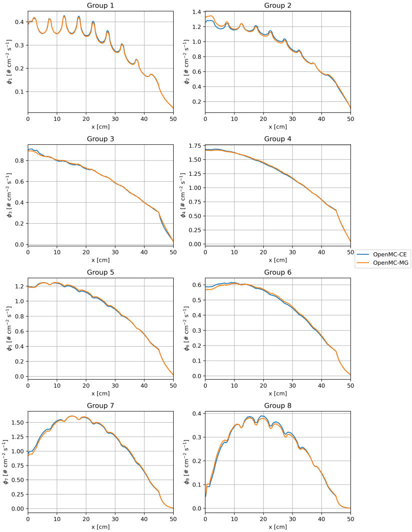

Figure 16: Case 3b neutron group flux distributions from OpenMC-CE and OpenMC-MG.

Case 3a Neutron Flux Distributions

- The neutron diffusion and hybrid methods fare worse than the S_8 method at capturing the oscillatory flux pattern.
- The hybrid method performs better than the neutron diffusion method near $x = 0$ cm where the correction region is situated.

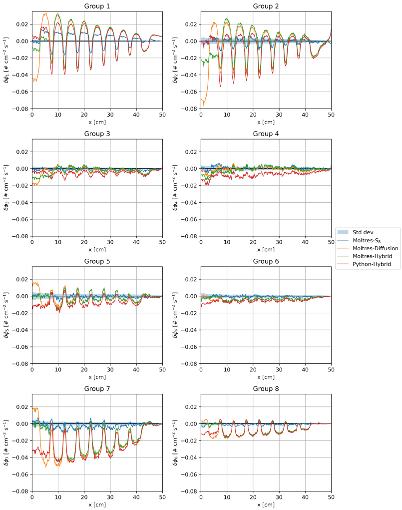

Figure 17: Absolute difference in neutron group flux distributions for Case 3a from Moltres-S_8, Moltres-diffusion, Moltres-hybrid, and Python-hybrid relative to OpenMC-MG.

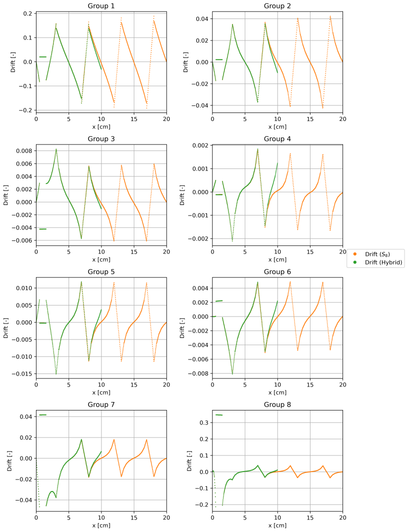

Figure 18: Multigroup drift correction ($\vec{D}_g$) x-component distributions from the Moltres-hybrid and Moltres-S_8 solvers.

Hybrid S_N-Diffusion Method: 1-D Neutronics Eigenvalue Simulations

Impact of Correction Subregion Sizes on k

- Minimizing the correction region size is essential for the hybrid method to be computationally efficient for time-dependent simulations.
- k varies by up to 164 pcm for Case 3a and 109 pcm for Case 3b.
- The hybrid method k value does not converge monotonically towards the S_8 method k value, implying other sources of discrepancies.

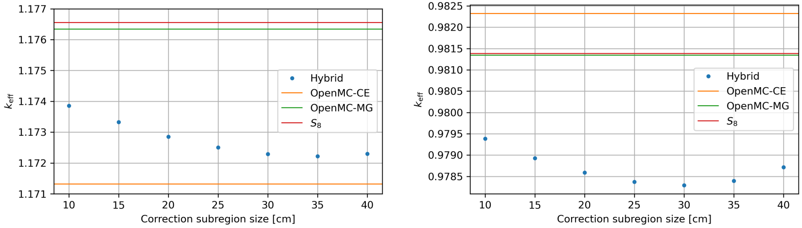

(a) Case 3a (b) Case 3b

Figure 19: k_{eff} estimates from the hybrid method for Cases 3a and 3b with different correction subregion sizes. The horizontal lines indicate k_{eff} estimates from the OpenMC-CE, OpenMC-MG, and S_8 methods.

2-D Neutronics Quarter-Core & Full-Core MSRE Models

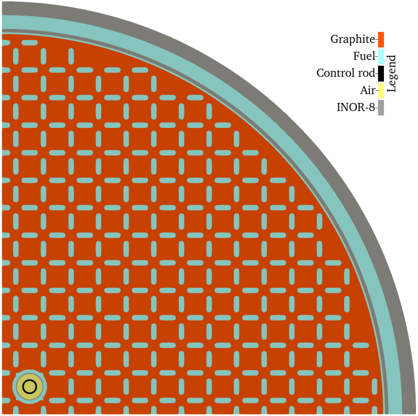

Figure 20: 2-D MSRE quarter-core model based on the horizontal cross section of the actual MSRE geometry.

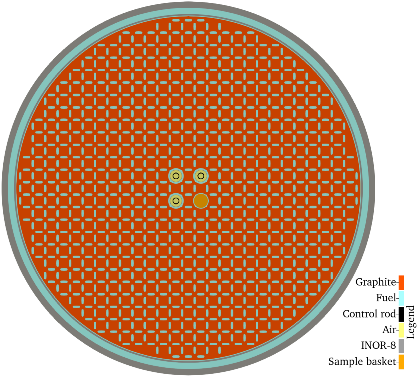

Figure 21: 2-D MSRE full-core model based on the horizontal cross section of the actual MSRE geometry.

2-D MSRE Neutronics Simulation Results

2-D Quarter-Core *k* & Rod Worth Results

Table 3: k_{eff} and control rod worth estimates for the 2-D quarter-core MSRE model. Error values are relative to OpenMC-CE.

Method	No Rod		Rod		Rod worth	
	k_{eff}	Error [pcm]	k_{eff}	Error [pcm]	$\Delta\rho_{worth}$ [pcm]	Error [pcm]
OpenMC-CE	1.112 09(43)	-	1.017 40(42)	-	8370(53)	-
OpenMC-MG	1.119 79(42)	618	1.022 04(41)	446	8541(51)	172
Diffusion	1.120 59	682	1.009 03	−816	9867	1484
Hybrid	1.121 74	773	1.025 32	760	8383	13

⇒ The hybrid method produces accurate rod worth estimates while the neutron diffusion method significantly overestimates rod worth.

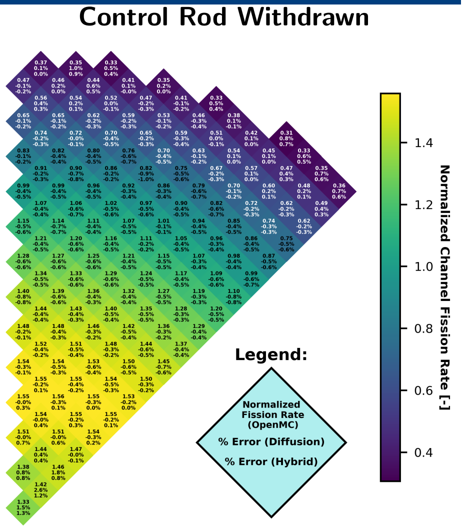

Figure 22: Normalized channel fission rate distribution of the 2-D MSRE quarter-core model with the rod withdrawn.

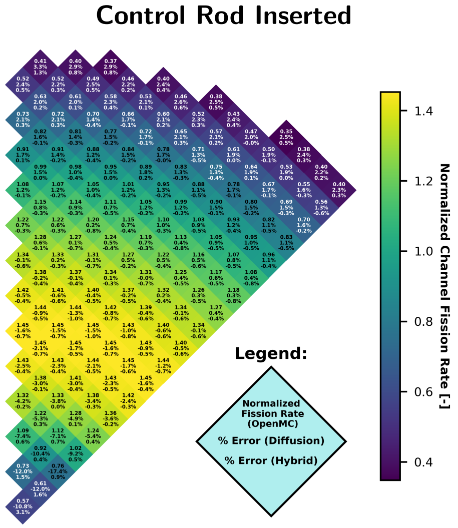

Figure 23: Normalized channel fission rate distribution of the 2-D MSRE quarter-core model with the rod inserted.

2-D MSRE Neutronics Simulation Results

2-D Quarter-Core Normalized Channel Fission Rate Distribution

Table 4: Absolute mean and maximum percentage errors in the normalized channel fission rates of the 2-D MSRE quarter-core models relative to OpenMC. The mean relative standard deviation of OpenMC normalized channel fission rates is 0.20%.

Method	No Rod		Rod	
	Mean [%]	Maximum [%]	Mean [%]	Maximum [%]
Diffusion	0.40	2.63	2.01	17.44
Hybrid	0.40	1.32	0.43	3.08

- The hybrid method improves channel fission rate estimates, especially for the rodded case.
- Significant improvement in maximum percentage error of the channel fission rate.

2-D MSRE Neutronics Simulation Results

2-D Full-Core Rod Worth Results

Table 5: Control rod worth estimates for the 2-D full-core MSRE with the indicated rods inserted. Error values are relative to OpenMC-CE.

Method	Rod 1		Rod 1 & 2		Rod 1, 2 & 3	
	$\Delta\rho_{\text{worth}}$ [pcm]	Error [pcm]	$\Delta\rho_{\text{worth}}$ [pcm]	Error [pcm]	$\Delta\rho_{\text{worth}}$ [pcm]	Error [pcm]
OpenMC-CE	2450(25)	-	4494(23)	-	6357(24)	-
OpenMC-MG	2523(23)	73	4640(24)	146	6455(22)	98
Diffusion	3019	569	5439	945	7519	1162
Hybrid	2455	5	4521	27	6323	-34

$\Rightarrow$ The hybrid method remains effective at improving control rod worth estimates in the full-core model.

2-D MSRE Neutronics Simulation Results

2-D Full-Core Normalized Channel Fission Rate Distribution

Table 6: Absolute mean and maximum percentage errors in the normalized channel fission rates of the 2-D MSRE full-core models relative to OpenMC. The mean relative standard deviation of OpenMC normalized channel fission rates is 0.27%.

Method	No Rod		Rod 1		Rod 1 & 2		Rod 1, 2 & 3	
	Mean [%]	Maximum [%]	Mean [%]	Maximum [%]	Mean [%]	Maximum [%]	Mean [%]	Maximum [%]
Diffusion	0.45	2.95	0.94	12.61	1.35	15.34	1.67	17.09
Hybrid	0.43	1.45	0.43	1.82	0.43	2.26	0.43	2.52

- Mean percentage error for the hybrid method remains consistent at 0.43%.
- Significant improvement in maximum percentage error of the channel fission rate.

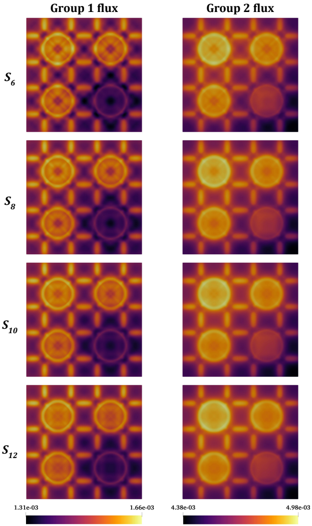

Figure 24: Group 1 and 2 neutron flux distributions in the hybrid S_N-diffusion method correction region with S_6, S_8, S_{10}, & S_{12}.

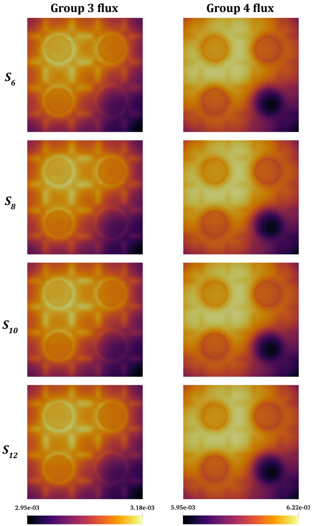

Figure 25: Group 3 and 4 neutron flux distributions in the hybrid S_N-diffusion method correction region with S_6, S_8, S_{10}, & S_{12}.

3-D MSRE Full-Core Model

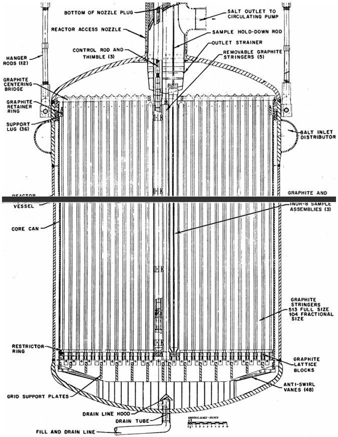

Figure 26: Vertical cross section of the actual MSRE vessel.

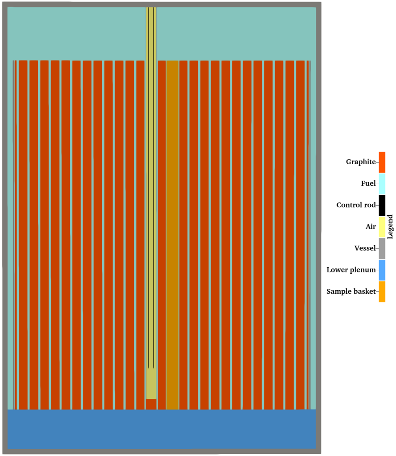

Figure 27: Vertical cross section of the 3-D numerical MSRE model offset by 5.08 cm to show the control rod thimble and homogenized sample basket.

3-D MSRE Neutronics Modeling Approach

3-D Full-Core MSRE Model Details

- Hybrid S_6-diffusion method
- Eight neutron energy groups
- ^{235}U concentration at initial criticality
- Uniform temperature at 911 K

All hybrid method results are compared with MSRE experimental data, the MSRE numerical benchmark report data (Serpent 2 model) [16], and the OpenMC model in this work.

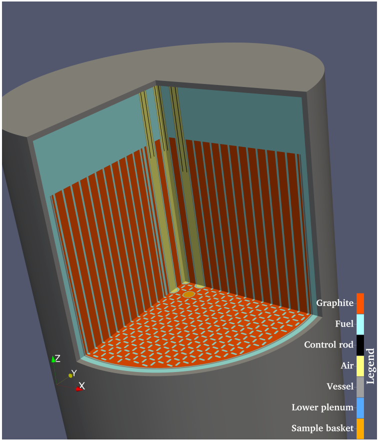

Figure 28: 3-D section view of the 3-D numerical MSRE model showing the three control rod thimbles and the fuel-graphite lattice.

3-D MSRE Neutronics Simulation Results

MSRE at Initial Criticality

Table 7: k_{eff} values from MSRE experimental data, the MSRE numerical benchmark [16], and the OpenMC and Moltres models in this work.

Source	k_{eff}
MSRE experimental data	1.000 00(420)
Serpent 2 (Numerical benchmark)	1.021 32(3)
OpenMC (This work)	1.013 08(20)
Hybrid (This work)	1.019 57
Diffusion (This work)	1.018 85

$\Rightarrow$ The hybrid and neutron diffusion models agree with the Serpent 2 and OpenMC models within 700 pcm.

3-D MSRE Neutronics Simulation Results

MSRE Rod Worth Measurements

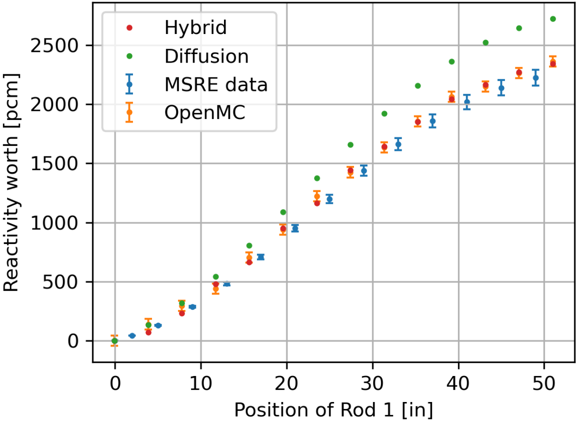

Figure 29: Reactivity inserted by Rod 1 at various rod positions relative to the full insertion.

3-D MSRE Neutronics Simulation Results

Strong Scaling Test

Performed a strong scaling test on the 3-D quarter-core MSRE model on 10, 20, 40, and 80 compute nodes. The S_N and diffusion subsolvers scale well throughout the test. The S_N-diffusion data transfer processes scale poorly beyond 40 nodes.

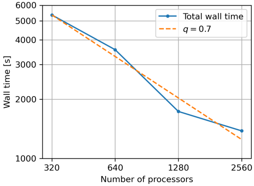

(a) Total wall time

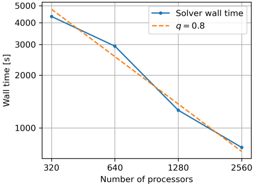

(b) Solver wall time

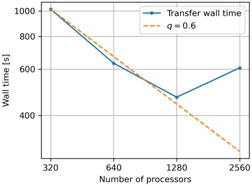

(c) Transfer wall time

Figure 30: The total, solver, and transfer wall time of hybrid method simulations of the 3-D quarter-core model on 10, 20, 40, and 80 compute nodes (32 processors per node) of the Polaris supercomputer. All axes are in log scale.

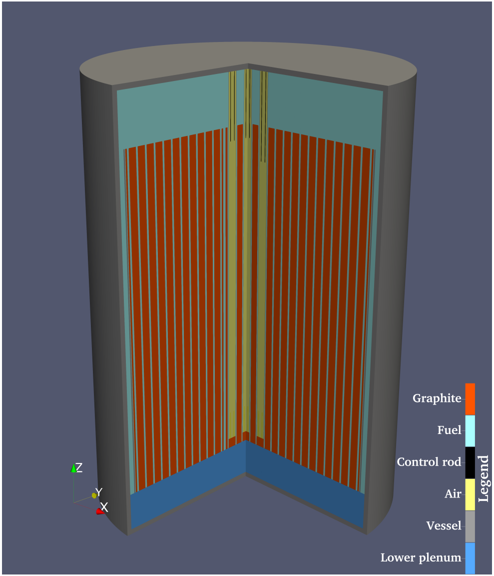

Figure 31: 3-D section view of the MSRE model geometry with Rod 1 inserted by 4.4 inches at initial criticality.

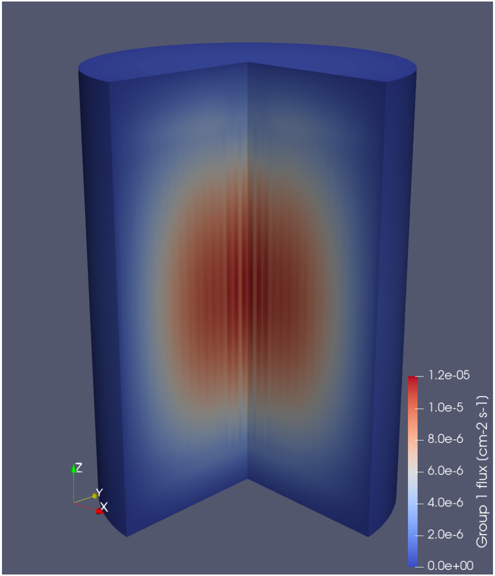

Figure 32: Group 1 neutron flux distribution with Rod 1 inserted by 4.4 inches at initial criticality.

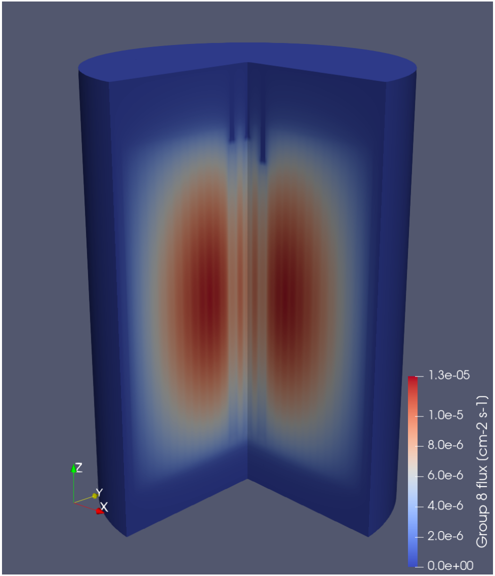

Figure 33: Group 8 neutron flux distribution with Rod 1 inserted by 4.4 inches at initial criticality.

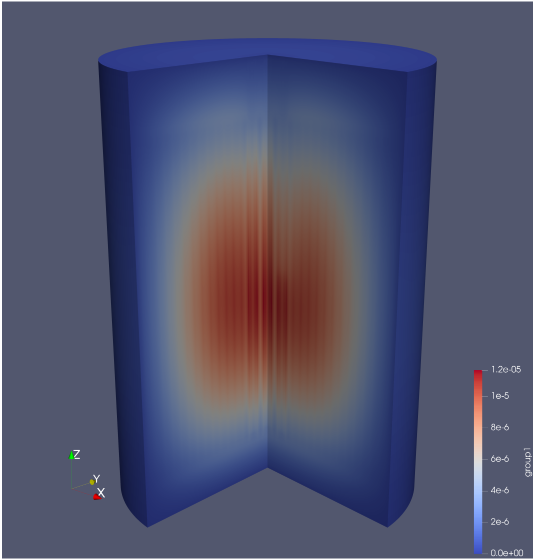

Figure 34: Group 1 neutron flux distribution with Rod 1 inserted by 27.5 inches.

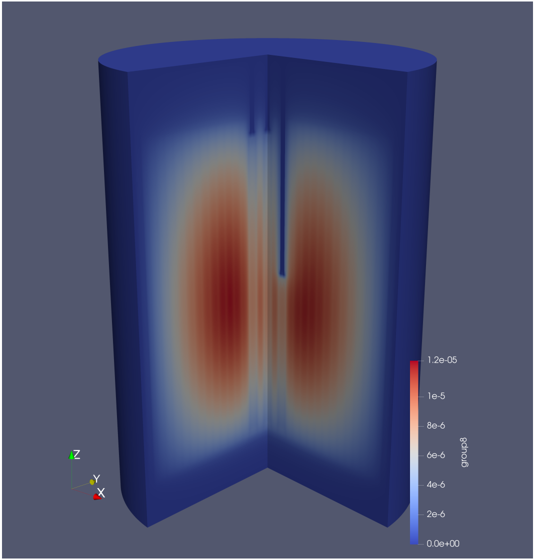

Figure 35: Group 8 neutron flux distribution with Rod 1 inserted by 27.5 inches.

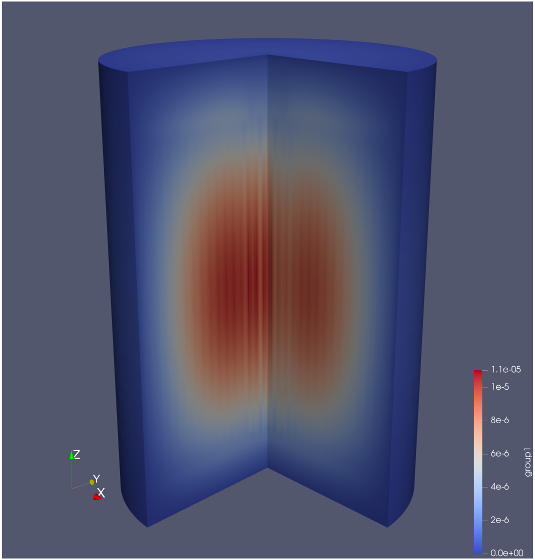

Figure 36: Group 1 neutron flux distribution with Rod 1 inserted by 51 inches.

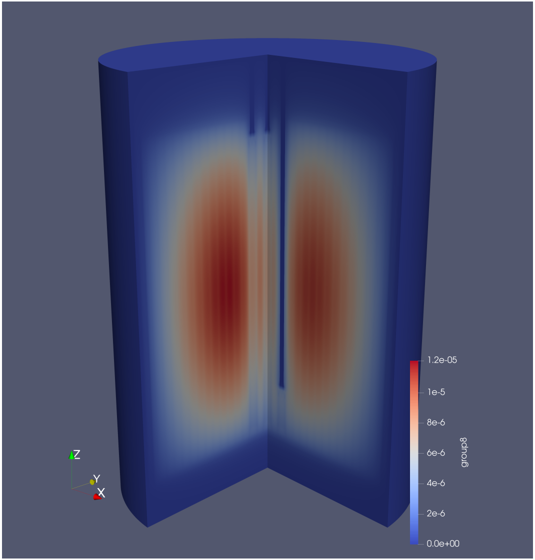

Figure 37: Group 8 neutron flux distribution with Rod 1 inserted by 51 inches.

Time-Dependent Simulations with the Hybrid Method

Time-dependent reactivity-initiated simulation based on an MSRE rod drop experiment.

MSRE Rod Drop Experiment

- Neutronic response of an initially critical, zero-power MSRE to a rod drop of Rod 1 [17]
- Corresponds to a reactivity withdrawal of -1500 pcm
- Requires delayed neutron precursor (DNP) modeling
- Induces a prompt response, followed by a delayed response, in the neutron count rate

MSRE Rod Drop Simulation Results

Neutron Count Rate Following Rod Drop

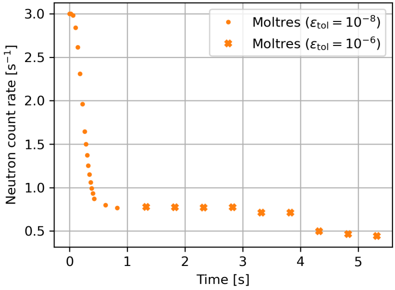

Figure 38: Neutron count rate during the rod drop experiment from Moltres rod drop simulation.

- Steep initial decline in neutron count rate as the rod drops
- Decline in neutron count rate slows at $t = 0.5$ s due to presence of DNPs
- Convergence issues prevented the simulation from converging from $t = 0.8$ s
- Raised the convergence tolerance value after $t = 0.8$ s to help the simulation continue

MSRE Rod Drop Simulation Results

Integral Neutron Count Following Rod Drop

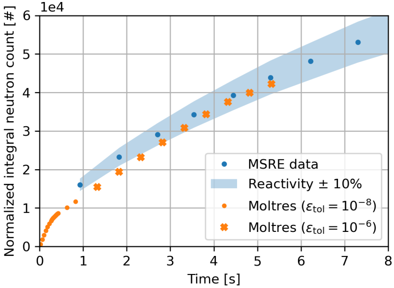

Figure 39: Integral neutron count during the rod drop experiment from MSRE experimental data and hybrid method numerical results.

- Moltres reproduces the expected trend in the integral neutron count rate.
- Slight underprediction relative to MSRE rod drop experimental data
- Underprediction may be due to experimental uncertainty in ^{235}U concentration, initial & final rod height, initial neutron count rate.

3-D Modeling with the Hybrid Method

Difficulties Faced During 3-D Modeling

- Slow convergence rate relative to 1-D & 2-D modeling
  - Likely due to increased streaming effects in 3-D near-void (air) regions in the reactor
- Significant memory requirements
- Lagged control rod positions in fixed point iterations affecting convergence in time-dependent simulations $\Rightarrow$ simulation requires smaller timestep sizes

MSRE Rod Drop Simulation Interpolated Results

Neutron Count Rate

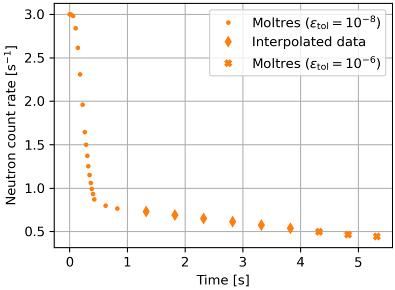

Figure 40: Neutron count rate during the rod drop experiment with linearly interpolated data between $t = 1.325$ s and $t = 3.825$ s.

Integral Neutron Count

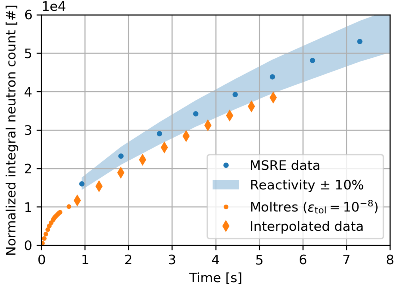

Figure 41: Integral neutron count during the rod drop experiment with linearly interpolated count rate data between $t = 1.325$ s and $t = 3.825$ s.

Rod Cusping Correction

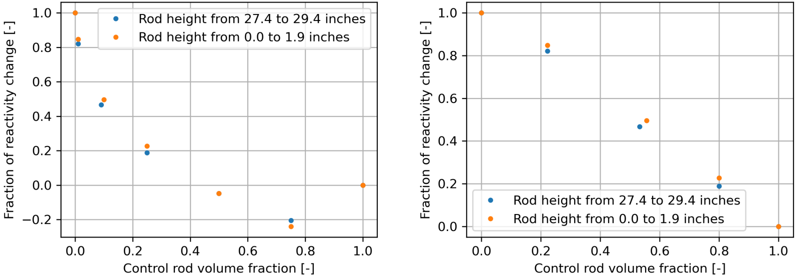

(a) Uncorrected volume weighting

(b) Corrected volume weighting

Figure 42: Fraction of reactivity change against control rod volume fraction in mixed mesh elements with the rod inserted at mid-reactor height (27.4 to 29.4 inches) and full insertion height (0.0 to 1.9 inches).